ORTHOGONAL POLARIMETRIC SAR PROCESSOR BASED ON SIGNAL AND INTERFERENCE SUBSPACE MODELS

F. Brigui[*]*, L. Thiron-Lefevre*

Supélec, Sondra, France

G. Ginolhac, P. Forster

ENS Cachan, Satie UniverSud, France

1. INTRODUCTION

Detection of target in complex environment is a current issue in SAR community. For FoPen (Foliage Penetration) applications, many scatterers cause false alarms. To increase detection in such environment, SAR processors using the properties of the scattering of the target have been developed [1, 2]. Nevertheless, false alarms still remain as long as their scattering have common properties to that of the target. In this study, we propose a new SAR processor to reduce these false alarms. We first consider the part of the interference scattering that is different from the target scattering. Then, we estimate this part of scattering and process an image in which only the interferences have a response. In order to reduce false alarms, this image is then combine with an image in which the target is detected [1, 2]. Results on simulated data for FoPen application show the interest of this method.
The following convention is adopted : italic indicates a scalar quantity, lower case boldface indicates a vector quantity and upper case boldface a matrix. T denotes the transpose operator and † the transpose conjugate.

2. PROBLEM STATEMENT

2.1. SAR Configuration and Notations

In SAR configuration, we consider that an antenna evolves along a linear trajectory ; at each position u_i, $i \in [\![1, N]\!]$ the antenna emits a signal and receives the response from the scene under observation. For more details on SAR configuration and process see [3]. The distance between adjacent positions is constant and equal to δu. The emitted signal is a chirp in polarization H ($p = H$) or V ($p = V$) with a frequency bandwidth B, a central frequency f_0 and a duration T_e. We denote by $\mathbf{z}_{pi} \in \mathbb{C}^K$ ($i \in [\![1, N]\!]$) the received signal samples at every u_i position of the antenna either in horizontal polarization or in vertical polarization and K is the number of time samples. The total received signal $\mathbf{z}_p$ for one polarization channel is the concatenation of the N vectors $\mathbf{z}_{pi}$ (see [1]) :

$$\mathbf{z}_p \in \mathbb{C}^{NK}, \quad \mathbf{z}_p = \begin{bmatrix} \mathbf{z}_{p1}^T & \mathbf{z}_{p2}^T & \dots & \mathbf{z}_{pN}^T \end{bmatrix}^T \tag{1}$$

The total polarimetric received signal $\mathbf{z}$ is then the concatenation of $\mathbf{z}_H$ and $\mathbf{z}_V$:

$$\mathbf{z} \in \mathbb{C}^{2NK}, \quad \mathbf{z} = \begin{bmatrix} \mathbf{z}_H^T & \mathbf{z}_V^T \end{bmatrix}^T \tag{2}$$

We precise that only the co-polarized channels are considered ($H = HH$ and $V = VV$).

2.2. Problem Modeling

We consider that a MMT (man-made target) is located at the pixel $t = (x_t, y_t)$ and an interference is located at the pixel $c = (x_c, y_c)$. For clarity of presentation, only one target and one interference are considered but the case of several scatterers is straightforward. To take into account the physical properties of the target scattering, we assume that a MMT can be modeled by a set of Perfectly Conducting (PC) plates having each one a different orientation described by the angles (α, β). The same idea is applied to describe the scattering of the interference. As for FoPen applications in P-band the false alarms are mainly due to the trunks of trees, the interference is modeled by a dielectric cylinder whose orientation is described by the angles (γ, δ). The orientations (α, β) and (γ, δ) of the target and the interference are unknown. As these latter strongly influence the scattering

[*]Thanks to DGA (Direction Générale de l'Armement) for funding.

pattern of the target and the interference, we can not favor a single orientation. Thus our models have to take into account all the possible orientations of a target or an interference. We assume then that for any orientation (α, β) of the PC plate and (γ, δ) of the dielectric cylinder, our models belong to a low-rank subspace, called $\langle H_{xy} \rangle$ for the target model and $\langle J_{xy} \rangle$ for the interference model (for more details on these subspaces and their generation, see for one polarimetric channel [1] and for co-polarized channels [2]). The modeling of $\mathbf{z}$ is written as :

$$\mathbf{z} = \mathbf{H}_t \boldsymbol{\lambda}_t + \mathbf{J}_c \boldsymbol{\mu}_c + \mathbf{n} \tag{3}$$

where $\mathbf{H}_t$ and $\mathbf{J}_c$ are respectively orthonormal bases of $\langle H_t \rangle$ and $\langle J_c \rangle$, $\boldsymbol{\lambda}_t$ and $\boldsymbol{\mu}_c$ are unknown coordinate vectors. $\mathbf{n}$ is a vector of white Gaussian noise of variance σ^2. The computation of the bases $\mathbf{H}_t$ and $\mathbf{J}_c$ are obtained from [4] and are detailed in [1, 2]. Knowing that $\mathbf{I} = \mathbf{P}_{\mathbf{H}_c} + \mathbf{P}^{\perp}_{\mathbf{H}_c}$ ($\mathbf{P}_{\mathbf{H}_c} = \mathbf{H}_c \mathbf{H}_c^{\dagger}$ and $\mathbf{P}^{\perp}_{\mathbf{H}_c} = \mathbf{I} - \mathbf{P}_{\mathbf{H}_c}$) the received signal $\mathbf{z}$ in Eq. (3) can be rewritten as follows :

$$\mathbf{z} = \mathbf{H}_t \boldsymbol{\lambda}_t + (\mathbf{P}_{\mathbf{H}_c} \mathbf{J}_c) \boldsymbol{\mu}_c^{\parallel} + (\mathbf{P}^{\perp}_{\mathbf{H}_c} \mathbf{J}_c) \boldsymbol{\mu}_c^{\perp} + \mathbf{n} \tag{4}$$

where $\boldsymbol{\mu}_c^{\parallel}$ and $\boldsymbol{\mu}_c^{\perp}$ are unknown coordinate vectors. The Eq. (4) allows us to separate the part $\boldsymbol{\mu}_c^{\parallel}$ of the scattering of the interference similar to the target scattering and to select only $\boldsymbol{\mu}_c^{\perp}$ to describe the interferences later on in this paper.

2.3. Hypotheses on $\mathbf{H}_t$ and $\mathbf{J}_c$

We express here two important hypotheses on the subspaces $\langle H_t \rangle$ and $\langle J_t \rangle$:

– Hypothesis 1
$\mathbf{H}_t^{\dagger} \mathbf{J}_t \neq \mathbf{0}$ (and $\mathbf{J}_t^{\dagger} \mathbf{H}_t \neq \mathbf{0}$).
The subspaces $\langle H_t \rangle$ and $\langle J_t \rangle$ are not necessarily orthogonal. This means that the signal of a target at t has a non-null projection on $\langle J_t \rangle$. We have the same hypothesis for the position c.

– Hypothesis 2
$\mathbf{H}_c^{\dagger} \mathbf{H}_t \neq \mathbf{0}$ and $\mathbf{J}_t^{\dagger} \mathbf{J}_c \neq \mathbf{0}$ but, $\|\mathbf{H}_c^{\dagger} \mathbf{H}_t \boldsymbol{\lambda}_t\| \approx 0$, $\|\mathbf{J}_t^{\dagger} \mathbf{J}_c \boldsymbol{\mu}_c\| \approx 0$. For two different positions (x_t, y_t) and (x_c, y_c), the subspaces $\langle H_t \rangle$ and $\langle H_c \rangle$ (or $\langle J_t \rangle$ and $\langle J_c \rangle$) are not necessarily orthogonal. Nevertheless the parameters $\boldsymbol{\lambda}_t$ and $\boldsymbol{\mu}_c$ in this case have an almost null-projection onto subspaces corresponding to different positions : we can distinguish the signal of two scatterers at different positions (x_t, y_t) and (x_c, y_c). This hypothesis is verified a posteriori in the SAR images in Section 4.
In the same way, we have $\|\mathbf{J}_c^{\dagger} \mathbf{H}_t \boldsymbol{\lambda}_t\| \approx 0$, $\|\mathbf{H}_t^{\dagger} \mathbf{J}_c \boldsymbol{\mu}_c\| \approx 0$.

3. SAR IMAGE PROCESSORS

To process images, we first have to estimate the parameters $\boldsymbol{\lambda}_t$ and $\boldsymbol{\mu}_c^{\perp}$ in Eq. (4). From these estimations, we define for each pixel (x, y) the intensities of the different processors, one to detect the target and the other to detect the interference. Finally, we can combine these intensities to increase detection and reduce false alarms.

3.1. Estimation

To estimate the coordinate vectors $\boldsymbol{\lambda}_t$ and $\boldsymbol{\mu}_c^{\perp}$, we have to solve :

$$\begin{array}{rcl} \hat{\boldsymbol{\lambda}}_p & = & arg(\min_{\boldsymbol{\lambda}_t} \ \|\mathbf{z} - \mathbf{J}_c \boldsymbol{\mu}_c - \mathbf{H}_t \boldsymbol{\lambda}_t\|^2) \\ \hat{\boldsymbol{\mu}}_c^{\perp} & = & arg(\min_{\boldsymbol{\mu}_c^{\perp}} \ \|\mathbf{P}^{\perp}_{\mathbf{H}_c} \mathbf{z} - \mathbf{P}^{\perp}_{\mathbf{H}_c} \mathbf{H}_t \boldsymbol{\lambda}_t - (\mathbf{P}^{\perp}_{\mathbf{H}_c} \mathbf{J}_c) \boldsymbol{\mu}_c^{\perp}\|^2) \end{array} \tag{5}$$

Using the least square method, we obtain :

$$\begin{array}{rcl} \hat{\boldsymbol{\lambda}}_t & = & \mathbf{H}_t^{\dagger} \mathbf{z} - \mathbf{H}_t^{\dagger} \mathbf{J}_c \boldsymbol{\mu}_c \\ \hat{\boldsymbol{\mu}}_c^{\perp} & = & (\mathbf{J}_c^{\dagger} \mathbf{P}^{\perp}_{\mathbf{H}_c} \mathbf{J}_c)^{-1} \mathbf{J}_c^{\dagger} \mathbf{P}^{\perp}_{\mathbf{H}_c} \mathbf{z} + (\mathbf{J}_c^{\dagger} \mathbf{P}^{\perp}_{\mathbf{H}_c} \mathbf{J}_c)^{-1} \mathbf{J}_c^{\dagger} \mathbf{P}^{\perp}_{\mathbf{H}_c} \mathbf{H}_t \boldsymbol{\lambda}_t \end{array} \tag{6}$$

From hypotheses in Section 2.3, we have :

$$\begin{array}{rcl} \hat{\boldsymbol{\lambda}}_t & = & \mathbf{H}_t^{\dagger} \mathbf{z} \\ \hat{\boldsymbol{\mu}}_c^{\perp} & = & (\mathbf{J}_c^{\dagger} \mathbf{P}^{\perp}_{\mathbf{H}_c} \mathbf{J}_c)^{-1} \mathbf{J}_c^{\dagger} \mathbf{P}^{\perp}_{\mathbf{H}_c} \mathbf{z} \end{array} \tag{7}$$

3.2. Signal and Orthogonal Interference Images

As we do not know the positions t of the target and c of the interference, we define the intensity for each pixel (x, y) of the signal image as the square modulus of $\boldsymbol{\lambda}_{xy}$ normalized by the noise variance and the intensity for each pixel (x, y) of the orthogonal interference image as the square modulus of $\boldsymbol{\mu}_{xy}^{\perp}$ normalized by the noise variance :

$$I_S(x,y) = \frac{\|\mathbf{H}_{xy}^{\dagger}\mathbf{z}\|^2}{\sigma^2} \ , \ I_{I\perp}(x,y) = \frac{\|\mathbf{J}_{xy}^{'\dagger}\mathbf{z}\|^2}{\sigma^2} \tag{8}$$

where $\mathbf{J}_{xy}^{'} = (\mathbf{J}_c^{\dagger}\mathbf{P}_{\mathbf{H}_c}^{\perp}\mathbf{J}_c)^{-1}\mathbf{J}_c^{\dagger}\mathbf{P}_{\mathbf{H}_c}^{\perp}$. In the image I_S, the target and the interference have a non-null response, however in the image $I_{I\perp}$ only the interference should appear.

3.3. Combination of I_S and $I_{I\perp}$

In the image I_S, it has been shown in [1, 2] that the target response is increased and the response of the white Gaussian noise is low. The image $I_{I\perp}$ provides us an image of the interferences. We can so combine the two images to increase the detection and to reduce false alarms. We propose a new SAR processor, the OSISDSAR (Orthogonal Signal and Interference Subspace Detector SAR) with the following intensity :

$$\begin{array}{lll} I_{SI}(x,y) = I_S(x,y) - \alpha I_{I\perp}(x,y) & \text{if} & I_S(x,y) - \alpha I_{I\perp}(x,y) \ \geq \ 0 \\ I_{SI}(x,y) = 0 & \text{if} & I_S(x,y) - \alpha I_{I\perp}(x,y) \ < \ 0 \end{array} \tag{9}$$

where α is a scale parameter between I_S and $I_{I\perp}$. In the image I_{SI}, the target has the same response as in the image I_S but the interferences are reduced. We propose one way to estimate α by solving the following equation :

$$\alpha = \arg(\min_{\alpha} \ \| \sum_{(x,y)} I_S(x,y) - \alpha \sum_{(x,y)} I_{I\perp}(x,y) \|^2) \tag{10}$$

The parameter α is then :

$$\alpha = \frac{\sum_{(x,y)} I_S(x,y)}{\sum_{(x,y)} I_{I\perp}(x,y)} \tag{11}$$

4. RESULTS

4.1. Configuration

To simulate a MMT for FOPEN applications, we simulate a metallic box on ground included in a simulated forest of trunks (see Fig. 1). The metallic box has a size of 2m x 1.5m x 1m and is located at the position $(110, -1, 0)$m ; its scattering is simulated with the commercial software FEKO [5] which takes into account all the scattering mechanisms (single and double bounce diffusion, edge effects). For the forest, only the trunks are simulated since they are the principal cause of the false alarms ; their scattering are simulated with COSMO [6]. We consider a flight between the first position $u_1 = -50m$ and the

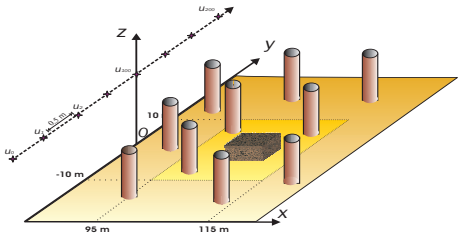

Fig. 1. SAR Configuration

last position $u_{200} = 50m$ with $\delta_u = 0.5m$ between each position and an altitude of $100m$. The full polarized emitted signal is a chirp with a central frequency of $400MHz$, a bandwidth of $100MHz$, and of duration $2.10^{-7}s$. Finally, the radar scene is defined in $[90, 140]m$ for x-axis and $[-25, 20]m$ for y-axis.

4.2. Images

To generate the bases $\mathbf{H}_{xy}$ and $\mathbf{J}_{xy}$ for processing the SDSAR and the OSISDSAR images, we choose a PC plate of size of $2mx1m$ and a dielectric cylinder of height of $11m$ and radius of $20cm$ for the model of the target and for the structured noise. The subspaces $\langle H_{xy} \rangle$ and $\langle J_{xy} \rangle$ have respectively a dimension of 6 and 10. In the Fig. 2(a), we present the SDSAR image ; the target is clearly detected but many false alarms due to the trees still remain. In the Fig. 2(b), we present the OSISDSAR image. The false alarms are widely reduced ; the polarimetric interference subspace describes their scattering even if only a part of it is used and permits us to have such result. We note that the response of the target is slightly reduced but remains high.

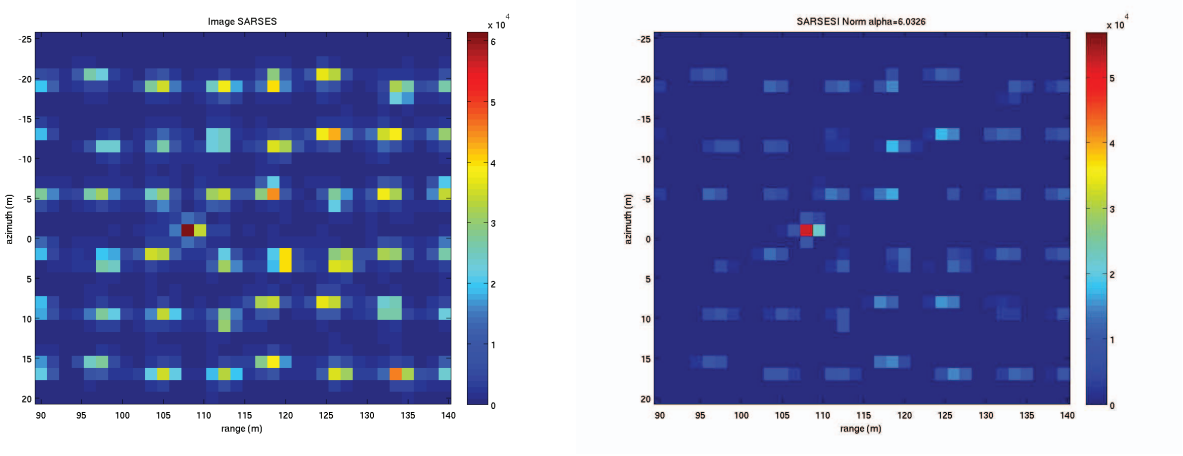

(a) (b)

Fig. 2. (a) SDSAR Image. (b) OSISDSAR Image.

5. CONLUSION

We have presented in this paper a new SAR processor, the OSISDSAR ; the scattering properties of target are used to increase detection while those of the interference are used to reduce false alarms. The main contribution of this study is to only consider the discriminative scattering properties of the interference to process an image in which there is no target response. The combination of the signal and interference image provides us a SAR processor for detection and false alarm reduction and its performance is evaluated on FoPen simulated data. We clearly show that the OSISDSAR outperforms the SDSAR in the reduction of false alarms. For future work, we want to work on the definition of the parameter α and relate it to a physical signification. Then the performance of detection and false alarm can be computed in order to evaluate precisely the performance of the processor. Finally, we want to apply this processor to real data for FoPen applications.

6. REFERENCES

[1] R. Durand, G. Ginolhac, L. Thirion-Lefevre, and P. Forster, "New SAR processor based on matched subspace detector," *IEEE TAES*, vol. 45, no. 1, pp. 221 – 236, January 2009.

[2] F. Brigui, G. Ginolhac, P. Forster, and L. Thirion-Lefevre, "New polarimetric signal subpace detectors for SAR processors," in *ICASSP 2009 Tapei Taiwan*, April 2009.

[3] M. Soumekh, *Synthetic Aperture Radar Signal Processing*, Wiley - Interscience Publication, 1999.

[4] P. Forster, "Generalized rectification of cross spectral matrices for array of arbitrary geometry," *IEEE TSP*, vol. 49, no. 5, 2001.

[5] *Feko, User's Manual, EM Software and System*, 2004.

[6] L. Thirion, E. Colin, and C. Dahon, "Capabilities of a forest coherent scattering model applied to radiometry, interferometry and polarimetry at p and l bands," *IEEE TGRS*, vol. 44, no. 4, 2006.